

On the importance of low-frequency modes
in predicting phase transitions
at high-pressure

Anna Hoser, Aleksandra Zwolenik, Anna Makal,
contact: *am.makal@uw.edu.pl*

May 30, 2024

Contents

S1 Methods	S2
S1.1 Crystallizations	S2
S1.2 Melting point determination	S2
S1.3 X-ray diffraction experiments	S3
S1.3.1 X-ray diffraction experiments at atmospheric pressure	S3
S1.3.2 High-pressure experiments	S3
S1.3.3 Structure solution and refinements	S5
S1.4 Deposition	S6
S1.5 Theoretical Calculations	S6
S1.6 Thermodynamic characteristics	S7
S1.7 Normal Mode Refinement (NoMoRe)	S8
S2 Crystal Structures of new polymorphs	S25
S2.1 Crystal structures of 2'AP polymorphs	S25
S2.1.1 Evolution of crystal structures of 2'AP with increased pressure	S27
S3 Lattice interactions	S30
S3.1 The most important intermolecular interactions	S30

Chapter S1

Methods

S1.1 Crystallizations

All di-acetyl-pyrene substrates for crystallizations were provided by dr Anna Wrona-Piotrowicz from the Chemistry Department of the University of Łódź. Crystals of 2["]AP and 2°AP- α have been obtained using the formerly applied protocols[1, 2].

Single crystals of the new 2°AP- β polymorph of the quality suitable for the single-crystal X-ray diffraction analysis could only be obtained by melting crystals 2°AP- α and slowly cooling them according to the procedure described elsewhere[3].

Recrystallization of 2'AP from a saturated solution in 1:1 mixture of dichloromethane and *n*-pentane yielded mainly good quality yellow block crystals of the known polymorph α . On the other hand, recrystallization by slow evaporation of the saturated solution of 2'AP in pure chloroform in a fridge ($\approx 15^\circ\text{C}$) yielded darker-yellow plates which proved to be exclusively the new β form.

S1.2 Melting point determination

Determination of the melting point temperatures was performed for single crystals of all the polymorphs of all di-acetyl-pyrenes at atmospheric pressure. The purity and quality of each crystal was confirmed by a short X-ray diffraction experiment (unit cell determination). Similarly-sized single crystals were placed on a siliconized glass wafer on a LinkamScientific TMS94 hot stage and then slowly heated at a rate of 2°C/min in air under a microscope. Such procedure was repeated twice on fresh single crystals. The melting point temperatures observed for the formerly described α polymorphs of di-acetyl-pyrene isomers were in excellent agreement with the former observations by Rajagopal et al.[4] within 2°C.

Melting points for polymorphs of 2°AP compound were also redetermined using the MP70 Melting Point System capillary apparatus (Mettler Toledo) with the heating rate of 5°C/min. The results were within 1°C of the observations for single-crystals.

S1.3 X-ray diffraction experiments

S1.3.1 X-ray diffraction experiments at atmospheric pressure

Low-temperature XRD diffraction data used for structure determination and further NoMoRe refinements were collected using the Rigaku Oxford Diffraction SuperNova 4-circle diffractometers equipped with either molybdenum or copper microsource and either Eos CCD detector or direct-counting HyPix detector (for 2°AP), and a LN2 cooling-device. Data collection and reduction was performed in CrysAlisPro[5]. Shape-based and empirical absorption correction were applied through the same software, using SCALE3 ABSPack. Further details of the procedures can be found in Tables S1.1 and S1.2.

Table S1.1: Data reduction and refinement details for 2'AP.

Temperature [K]	2'AP- α 100(2)	2'AP- α 280.10(10)	2'AP- β 100(2)	2'AP- β 280(2)
Empirical formula	$C_{20}H_{14}O_2$	$C_{20}H_{14}O_2$	$C_{20}H_{14}O_2$	$C_{20}H_{14}O_2$
Formula weight [$\frac{g}{mol}$]	286.31	286.31	286.31	286.31
Crystal system	monoclinic	monoclinic	monoclinic	monoclinic
Space group	P 1 21/n 1	P 1 21/n 1	P 1 21/c 1	P 1 21/c 1
a [Å]	9.2009(4)	9.2316(2)	8.02950(10)	8.12030(10)
b [Å]	7.3090(3)	7.44094(15)	23.1438(4)	23.1408(4)
c [Å]	10.0763(5)	10.0891(2)	7.45590(10)	7.56240(10)
α [°]	90	90	90	90
β [°]	98.993(5)	98.8945(19)	95.865(2)	95.1960(10)
γ [°]	90	90	90	90
Volume [Å ³]	669.30(5)	684.71(2)	1378.30(4)	1415.21(4)
Z	2	2	4	4
ρ_{calc} [$\frac{g}{cm^3}$]	1.421	1.389	1.380	1.344
μ [mm ⁻¹]	0.722	0.705	0.701	0.683
F(000)	300	300	600	600
Crystal size [mm ³]	0.35 x 0.19 x 0.05	0.32 x 0.21 x 0.18	0.27 x 0.18 x 0.09	0.33 x 0.19 x 0.05
Radiation source	CuK α	CuK α	CuK α	CuK α
Radiation wavelength [Å]	1.54184	1.54184	1.54184	1.54184
2θ range	12.118 to 143.226	12.098 to 155.02	7.64 to 156.34	7.64 to 155.416
Reflections collected	3928	5826	16650	13641
R_{int}	0.0186	0.0253	0.0423	0.0212
Resolution [Å]	0.8124	0.7896	0.7876	0.7890
Completeness	0.997	0.999	1.000	0.999
Data; restraints; parameters	1286; 0; 101	1450; 0; 101	2904; 0; 202	2998; 0; 202
$R_1(I > 2\sigma(I))$	0.0400	0.0467	0.0467	0.0529
$wR_2(I > 2\sigma(I))$	0.1081	0.1430	0.1414	0.1740
R_1 (all data)	0.0445	0.0503	0.0522	0.0613
wR_2 (all data)	0.1129	0.1462	0.1477	0.1839
Largest diff. peak [eÅ ⁻³]	0.284	0.236	0.493	0.322
Largest diff. hole [eÅ ⁻³]	-0.220	-0.257	-0.285	-0.196

Reference XRD data at room temperature for structure determinations at increased pressures were collected using the Rigaku Oxford Diffraction SuperNova 4-circle diffractometer equipped with HyPix detector, copper microsource (CuK α , $\lambda = 1.54184$ Å), and an LN2 cooling-device.

Crystals were mounted on Mitegen loops with a trace of ParatoneN oil.

S1.3.2 High-pressure experiments

Collecting X-ray diffraction data at increased pressures required samples of 2°AP- β , 2'AP- α and 2'AP- β to be placed in a Diamond Anvil Cell (DAC). Depending on

Table S1.2: Data reduction and refinement details for 2° AP- β .

Temperature [K]	2°AP- β
Empirical formula	100.00(10)
Formula weight [$\frac{g}{mol}$]	$C_{20}H_{14}O_2$
Crystal system	286.31
Space group	monoclinic
a [Å]	P 1 21/c 1
b [Å]	7.15110(13)
c [Å]	10.90793(19)
α [°]	17.7744(3)
β [°]	90
γ [°]	102.4944(19)
Volume [Å ³]	90
Z	1353.63(4)
ρ_{calc} [$\frac{g}{cm^3}$]	4
μ [mm ⁻¹]	1.405
F(000)	0.090
Crystal size [mm ³]	600
Radiation source	0.173 x 0.141 x 0.036
Radiation wavelength [Å]	Mo K α
2θ range	0.71073
Reflections collected	6.652 to 69.134
R_{int}	48392
Resolution [Å]	0.0488
Completeness	0.6263
Potency	0.998
Data; restraints; parameters	Not calculated
R_1 ($I > 2\sigma(I)$)	5486; 0; 255
wR_2 ($I > 2\sigma(I)$)	0.0440
R_1 (all data)	0.1198
wR_2 (all data)	0.0631
Largest diff. peak [eÅ ⁻³]	0.1293
Largest diff. hole [eÅ ⁻³]	0.471
	-0.194

the experimental attempt a single crystal of the investigated substance would be placed either in a) a Merill-Basset Diamond Anvil Cell with culet size of 750 μm and effective opening angle of 40 ° or b) an Almax DACOne20 diamond anvil cell with culet size of 500 μm and effective opening angle of over 50 deg. A 200 μm thick steel gaskets with hole diameter adjusted to the culet size were used and a ParatoneN oil or a low-density silicone oil was applied as a pressure-transmitting medium.

Pressure estimation utilized fluorescence from reference ruby spheres, one of which was inserted into a DAC alongside the sample in each high pressure experiment. The ruby signal was identified using an Almax Optiprexx PLS spectrometer, affording the nominal precision of 0.05 GPa. Position of the R1 peak was determined by means of fitting a pseudo-Voigt curve to the fluorescence spectrum using custom-made software pRuby[6]. The pressure was estimated based on calibration curve determined by Piermarini et al.[7]. Temperature correction was also applied[8].

Effective DAC opening angle cutoffs, smaller than the nominal aperture, were used for the sake of data processing, as the intensities of the few reflections registered beyond the effective limits were found to be heavily affected by gasket shadowing.

XRD data for structure determination for 2'AP- α and 2'AP- β at increased pressures were collected using the Rigaku Oxford Diffraction SuperNova 4-circle diffractometer equipped with Atlas CCD detector and molybdenum microsource (MoK α , $\lambda = 0.71073 \text{ \AA}$) at 295 K. A total of two interpretable datasets per each 2'AP poly-

Table S1.3: Parameters of DACs utilized in performed high pressure experiments.

	Modified Merrill-Bassett	DAC One20
Diameter of diamond cullet	0.75 mm	0.50 mm
Diameter of gasket hole	0.50 mm	0.30 mm
Nominal opening angle	40°	60°
Effective opening angle	30–35°	45–50°

morph were collected at pressures of ≈ 0.5 GPa and around 2.0 GPa.

A summary of obtained unit cell parameters and other experiment descriptors are listed in Table S1.4.

Table S1.4: Data reduction and refinement details for HP structures of 2'AP.

Pressure [GPa]	2'AP- α 0.56	2'AP- α 1.76	2'AP- β 0.51	2'AP- β 2.0
Empirical formula	$C_{20}H_{14}O_2$	$C_{20}H_{14}O_2$	$C_{20}H_{14}O_2$	$C_{20}H_{14}O_2$
Formula weight [$\frac{g}{mol}$]	286.31	286.31	286.31	286.31
Temperature [K]	291.15	290.15	287.15	292.15
Opening angle [°]	40	40	40	50
Crystal system	monoclinic	monoclinic	monoclinic	monoclinic
Space group	P 1 21/n 1	P 1 21/n 1	P 1 21/c 1	P 1 21/c 1
a [Å]	9.16(4)	9.03(4)	8.017(3)	7.901(2)
b [Å]	7.308(4)	7.104(4)	23.00(3)	22.685(5)
c [Å]	10.05(4)	9.88(4)	7.369(3)	6.897(11)
α [°]	90	90	90	90
β [°]	100.1(4)	101.4(5)	95.75(3)	96.68(5)
γ [°]	90	90	90	90
Volume [Å ³]	662(4)	621(4)	1352.1(18)	1228(2)
Z	2	2	4	4
ρ_{calc} [$\frac{g}{cm^3}$]	1.436	1.531	1.407	1.549
μ [mm ⁻¹]	0.092	0.098	0.090	0.099
F(000)	300	300	600	600
Crystal size [mm ³]	0.28 x 0.21 x 0.09	0.28 x 0.21 x 0.09	0.25 x 0.12 x 0.08	0.25 x 0.12 x 0.08
Radiation source	MoK α	MoK α	MoK α	MoK α
Radiation wavelength [Å]	0.71073	0.71073	0.71073	0.71073
2 θ range	5.556 to 52.392	5.588 to 52.474	5.406 to 65.458	5.19 to 52.742
Reflections collected	1922	2014	4593	4771
R_{int}	0.1386	0.1797	0.0685	0.1322
Resolution [Å]	0.8050	0.8038	0.6573	0.8000
Completeness (Laue full)	0.324	0.381	0.566	0.492
Data; restraints; parameters	414; 78; 102	462; 78; 102	1938; 108; 201	1204; 108; 202
$R_1(I > 2\sigma(I))$	0.0544	0.1269	0.1480	0.1015
$wR_2(I > 2\sigma(I))$	0.1206	0.3051	0.1628	0.2506
R_1 (all data)	0.1404	0.2367	0.3215	0.2403
wR_2 (all data)	0.1705	0.3888	0.2140	0.3586
Largest diff. peak [eÅ ⁻³]	0.142	0.225	0.166	0.278
Largest diff. hole [eÅ ⁻³]	-0.127	-0.261	-0.198	-0.209

In the case of 2'AP- β a series of high-quality single-crystal X-ray diffraction datasets suitable for structural analysis have been obtained at the CRISTAL beamline at SOLEIL synchrotron in France. They were performed at applied pressures of 0.85, 1.1 and 1.7 GPa. The results will be described in more detail elsewhere[3].

S1.3.3 Structure solution and refinements

The structures were solved using SHELXT and refined using olex2.refine coupled with NoSpherA2, using the TAAM approach, aspherical scattering factors being provided by DISCaMB[9–12].

The crystal structures at high-pressure for 2'AP were solved with either SHELXT or SHELXD, and further refined assuming spherical atomic scattering factors using SHELXL[9, 13, 14]. Structure solution and refinement were performed within the Olex2 GUI[15]. The reasonable completeness of the obtained data allowed all non-H atoms to be located from a Fourier map and refined assuming anisotropic Atomic Displacement Parameters with loose RIGU restraints. The hydrogen atom positions were constrained to their closest carbons and had their movement defined using the riding approximation (AFIX instruction in SHELX).

Molecular graphics were prepared using either Olex2[15] or Mercury 4.4 software[16].

S1.4 Deposition

Structures determined for the purpose of this paper were deposited as individual entries within Cambridge Structural Database[17]. Exact deposition number for each structure have been presented in Table S1.5.

Table S1.5: CCDC deposition numbers of crystal structures determined for the purpose of these studies, sorted by crystal phase and exerted pressure.

Polymer	T	Pressure	CCDC deposition number
2°AP- β	100K	atmospheric	2332704
	100K	atmospheric	2332703
	293K	atmospheric	2332701
	293K	0.5 GPa	2332700
	293K	1.8 GPa	2332696
2'AP- β	100K	atmospheric	2332699
	293K	atmospheric	2332698
	293K	0.5 GPa	2332697
	293K	2.0 GPa	2332702

S1.5 Theoretical Calculations

Periodic ab-initio density functional theory (DFT) calculations for investigated systems were performed using the CRYSTAL17[18]. The calculations used as ansatz for the Normal Mode Refinements (NoMoRe) were performed with the B3LYP functional in combination with D3 empirical dispersion[19, 20], which is widely used and provides reasonable relative stabilities for similar organic systems[21], as well as estimates of vibrational frequencies. A 6-31G(d,p) basis set was employed, the truncation parameters, TOLINTEG, were set to 7 7 7 7 25, and the shrinking factors in the reciprocal space, SHRINK, were set to 8 and 8. The geometry was optimized by adjusting only the coordinates from the experimental geometry with fixed unit cell parameters as derived from XRD experiments. The electronic energies per unit cell obtained at this stage (E_{ele}) were used as estimates of the electronic energy in

the assessment of Gibbs free energies. The lattice energies (E_{latt}) were estimated as a difference between total crystal energy per molecule and the energy of a single molecule in crystal-fixed geometry:

$$E_{latt} = E_{ele}/N - E_{molecule}$$

where N - number of molecules in the unit cell. Basis-set superposition corrections were applied[22]. Afterwards, normal modes and their frequencies were calculated at the Γ point of the Brillouin zone using the finite displacement method. To optimize the geometry, the convergence criteria were set to the default for frequency calculations, using the PREOPTGEOM keyword. Vibrational frequencies were calculated using the unit cell parameters derived from the XRD measurements. Input for CRYSTAL17 frequency calculations were produced using the cif2crystal routine[23].

S1.6 Thermodynamic characteristics

The electronic energies obtained from the periodic DFT calculations in combination with the vibrational frequencies derived from the normal mode refinements allowed to estimate the free energies of the polymorphs as a function of temperature, as have been done in previous work on dimethyl-3,6-dichloro-2,5-dihydroxyterephthalate and pyrazinamide. The free energy is derived as described in the following. Gibbs free energy is given by

$$G = H - TS \quad (\text{S1.1})$$

where H is enthalpy, T is temperature in K and S is entropy. The enthalpic part can be divided into:

$$H = U + p\Delta V \quad (\text{S1.2})$$

where U is a crystal packing energy and $p\Delta V$ is pressure multiplied by volume change, calculated at 1 atm. This division takes the expansion of the unit cell with temperature into account. Furthermore, U can be written as a sum of the electronic energy, which was obtained from the DFT calculations (E_{ele}), and the contribution from vibrational energy, which is equal to:

$$F_{vib} = \frac{1}{2} \sum_j h\nu_j + kT \sum_j \ln \left(1 - \exp \left(\frac{-h\nu_j}{kT} \right) \right) \quad (\text{S1.3})$$

where the summation includes frequencies ν , h is the Planck constant and k is the Boltzmann constant. The first part of this equation corresponds to the zero-point energy (ZPE) and the second part is the contribution to enthalpy (H_{vib}) related to normal-mode vibrations. Similarly, vibrational entropy can be written as:

$$S_{vib} = nR \sum_j \left(\frac{h\nu_j}{kT} \left(\exp \left(\frac{h\nu_j}{kT} - 1 \right)^{-1} - \ln \left(1 - \exp \left(\frac{h\nu_j}{kT} \right) \right) \right) \right) \quad (\text{S1.4})$$

which is a summation over all normal-mode vibrations. Final Gibbs free energies G were derived according to the formula:

$$G = E_{ele} + ZPE + H_{vib} + pV - TS_{vib} \quad (\text{S1.5})$$

Table S1.6: Summary of the thermodynamic properties of the investigated diacetyl-pyrene isomers at 293K. All energies are reported per single molecule of diacetyl-pyrene in kJ mol^{-1} . Relative differences in energy between polymorphs (Δ) were calculated by subtracting given energy of α from that of β , i.e. $\Delta E = E(\beta) - E(\alpha)$.

	2°AP		Δ	2°AP		Δ	2°AP		Δ
	CRYSTAL17 (Γ point)								
E_{ele}	-2417219.6	-2417221.9	-2.3	-2417233.7	-2417234.6	-0.9	-2417221.6	-2417219.9	1.7
ZPE	748.9	750.2	1.3	749.0	749.3	0.3	747.0	749.3	2.3
H_{vib}	46.2	44.7	-1.6	46.5	46.7	0.3	45.9	47.1	1.2
PV	0.0	0.0	0.0	0.0	0.0	0.0	0.0	0.0	0.0
TS_{vib}	89.3	84.7	-4.7	90.0	90.9	0.9	87.5	92.3	4.8
G	-2416513.8	-2416511.7	2.1	-2416528.3	-2416529.4	-1.2	-2416516.2	-2416515.8	0.4
Normal Modes Refinement									
5 lowest frequencies refined									
TS_{vib}	98.9	100.0	1.1	99.6	100.6	1.0	101.9	101.6	-0.3
G	-2416550.5	-2416553.0	-2.4	-2416565.1	-2416566.9	-1.8	-2416556.5	-2416553.0	3.5
12 lowest frequencies refined									
TS_{vib}	96.9	98.0	1.1	99.7	101.6	2.0	102.1	102.1	0.0
G	-2416548.4	-2416550.8	-2.4	-2416565.2	-2416567.9	-2.8	-2416556.7	-2416553.5	3.2

Frequencies taken directly from the periodic DFT calculations at the Γ -point were used for the initial calculation of H_{vib} and S_{vib} , and then non-refined vibrational modes were input into NoMoRe.

S1.7 Normal Mode Refinement (NoMoRe)

The NoMoRe program was used for the refinement of normal modes against the X-ray data. This was accomplished via the *nomore.chem.uw.edu.pl* web server. Normal-mode vectors and their frequencies were submitted as derived from the periodic DFT calculations. Together with results from calculations, structure factor amplitudes and structural models from single crystal X-ray diffraction measurements were submitted to NoMoRe. Frequencies for selected normal mode vectors were refined in order to minimize wR2 agreement factor. Various approaches were tested (by refining different subsets of vibrational frequencies), but due to correlations between the refined modes, it was decided to refine as low number of frequencies for low frequency modes as possible. Table S1.3 presents the subsets of refined frequencies in various approaches, together with the final obtained wR2 agreement factors. All the frequencies were used to estimate vibrational contributions to free Gibbs energy G. Frequencies higher than 500 cm^{-1} were scaled by factor 0.956 in order to correct for anharmonicity.

Table S1.7: Vibrational frequencies and wR² agreement factors from NoMoRe. Items in bold indicate final values of frequencies actually refined with NoMoRe approach. The remaining frequencies were obtained from periodic DFT calculations at Γ point only.

Value	2'AP- α			2'AP- β			2°AP- α			2°AP- β			2"AP- α			2"AP- β		
	N _{ref}	4	12	4	12	5	12	5	12	5	12	5	12	5	12	5	12	
wR ω [cm ⁻¹]	0.13	0.13	0.23	0.19	0.13	0.19	0.13	0.12	0.22	0.2	0.22	0.21	0.21	0.24	0.24	0.2	0.24	
18.809	19.323	19.606	11.703	70.608	74.993	32.927	35.767	9.995	10.709	12.015	21.797	21.334	50.424	173.269	33.101	65.137		
27.214	26.927	16.926	11.722	13.766	23.564	20.749	11.395	13.281	14.613	18.696	18.12	18.12	182.547	22.567	22.567	22.26		
31.537	32.39	84.459	28.883	35.065	40.488	21.79	24.432	21.789	25.746	24.432	34.501	28.427	29.702	23.433	23.433	20.448		
55.38	59.243	19.01	20.923	21.957	21.789	23.53	34.883	30.87	22.709	26.88	27.242	38.55	36.704	36.704	36.704	17.293		
56.55	35.321	26.2	12.653	21.493	32.9	33.259	32.32	16.919	31.55	24.007	51.25	106.812	59.78	57.652	29.15	27.097		
62.46	79.973	37.34	17.955	32.99	57.713	32.37	27.157	32.48	21.454	54.08	21.454	62.85	68.98	75.22	40.84	183.809	183.809	
76.04	72.903	48.04	26.042	35.64	49.697	41.07	32.22	38.02	27.585	65.79	124.431	82.4	99.531	48.31	47.01	57.516	92.764	
87.71	62.278	49.01	24.044	45.3	46.697	47.01	47.01	43.89	98.738	84.32	53.982	94.97	51.4	53.19	48.14	44.18	101.55	
94.97	51.54	54.4	53.35	53.35	53.35	53.35	53.35	53.35	51.73	51.73	103.38	95.85	55.61	62.6	48.76	55.35	105.87	
103.9	57.38	63.69	63.69	65.28	66.49	66.49	73.57	73.57	70.14	70.14	127.81	105.04	63.29	64.97	67.72	66.19	125.48	
110.24	64.97	64.97	66.99	69.12	70.06	70.06	77.39	77.39	72.37	72.37	127.02	115.01	69.14	69.83	74.53	81.11	151.98	
115.01	76.04	76.04	81.22	81.22	85.46	85.46	89.32	89.32	73.35	73.35	161.61	131.15	69.14	69.83	77.53	81.11	127.81	
131.15	79.46	81.98	81.98	83.03	95.19	95.19	104.14	104.14	92.79	92.79	149.85	131.41	82.49	82.49	83.32	104.14	225.15	
148.54	96.34	96.34	99.1	86.36	86.36	86.36	104.17	104.17	96.4	96.4	233.39	176.45	113.75	109.63	105.63	104.78	233.39	
178.51	100.23	105.45	97.58	97.58	105.66	105.66	108.5	108.5	108.35	108.35	242.37	197.64	160.87	162.45	162.45	116.16	123.81	
199.29	105.67	104.03	104.03	106.45	106.45	106.45	111.22	111.22	114.45	114.45	244.71	201.67	110.36	113.75	113.75	124.45	262.81	
220.38	128.42	132.44	132.44	131.82	142.48	142.48	144.54	144.54	133.33	133.33	287.97	275.13	132.16	132.16	132.16	126.14	290.86	
280.49																	305.57	

289.36	132.54	145.79	138.16	137.34
294.8	132.66	146.02	142.73	146.84
297.4	139.11	151.87	146.89	151.05
336.9	141.46	156.11	148.36	157.31
339.84	143	157.88	154.02	157.31
347.94	147.52	160.09	155.36	159.31
349.93	149.43	160.59	156.18	159.69
404.75	149.9	173.07	174.78	159.95
409.02	149.99	173.46	179.5	164.24
409.95	161.4	178.33	181.16	166.48
411.44	162.48	181.03	182.75	169.34
449.64	168.32	183.78	196.93	211.9
450.71	171.47	183.91	198.9	213.39
485.56	174.56	189.75	199.74	214.26
486.16	181.03	190.23	201.21	215.3
491.19	187.98	194	206.92	221.23
493.6	189.29	206.12	209.97	221.73
520.79	193.7	206.4	212.66	222.61
522.46	195.8	209.99	215.83	224.61
523.64	213.56	210.37	223.65	229.73
523.81	214.55	210.68	225.56	230.15
536.29	216.98	215.63	226.47	230.9
536.98	217.55	223.64	226.94	231.81
547.03	221.2	230.41	231.8	235.21
548.46	221.57	230.81	232.01	237.52
558.06	238.59	233.42	240.95	238.51
570.31	238.94	235.54	242.72	239.42
577.78	240.54	237.74	258.78	243.13
579.81	241.68	246.74	260.05	243.16
584.1	246.69	257.47	267.92	244.08
584.25	247.26	259.81	269	245.51
619.06	273.04	276.16	281.59	272.67
623.87	273.1	280.49	281.66	276.48
626.59	282.74	284.12	289.46	276.92
627.26	284.29	284.84	292.94	276.97
670.63	288.06	286.31	304.38	292.38
671.56	289.19	287.15	304.7	295.63
684.31	303.38	289.89	305.05	296.86
684.43	304.3	293.25	306.2	299.76
695.13	308.8	306.13	314.8	305.13
699.63	309.45	306.35	317.04	307.95
709.92	310.29	312.08	317.04	308.84
711.52	310.67	312.37	317.21	309.56
718.15	345.33	315.82	328.31	322.25

719.94	316.97	328.64	322.53
742.82	322.08	329.34	324.66
748.38	322.21	329.45	324.9
773.49	357.64	355.57	344.27
774.64	358.25	359.58	344.29
811.06	378.5	361.87	356.8
812.38	379.03	363.24	358.67
824.82	392.94	398.29	393.01
835.27	393.81	398.88	394.73
836.95	403.43	399.28	395.68
836.97	403.6	399.5	398.45
838.24	416.09	408.69	414.99
840.04	416.23	409.77	415.55
873.64	418.31	413.29	416.52
888.84	418.6	415.17	417.5
889.54	455.04	453.13	465.31
892.54	455.54	453.84	465.87
897.85	460.35	454.96	466.22
900.7	460.85	455.36	467.29
969.83	491.44	480.36	473.62
971.3	493.36	481.27	473.75
980.88	498.12	481.31	474.18
989.47	498.21	481.8	474.78
993.8	500.04	499.92	501.4
994.24	500.33	500.19	503.26
1005.25	504.69	500.53	504.13
1006.23	505.04	500.65	504.51
1012.53	514.47	500.95	504.71
1015.8	514.54	501.2	505.3
1016.53	517.25	505.35	506.04
1021.14	517.38	505.39	506.06
1021.43	522.81	518.71	513.54
1023.16	522.92	519.48	515.88
1044.14	526.06	526.56	519.84
1044.69	526.29	526.58	520.72
1048.04	543.23	530.33	530.43
1048.96	544.74	530.89	530.58
1081.26	546.29	531.86	530.93
1084.6	546.79	532.36	531.15
1135.95	547.35	540.18	542.24
1137.77	547.97	541.35	545.3
1158.99	550.94	545.08	548.14
1164.52	550.95	548.69	548.16
1168.1	567.69	553.1	557.83

1171.75	568.21	553.72	557.9	557.37
1190.86	573.31	554.56	557.98	558.16
1191.3	573.48	554.96	558.14	558.37
1203.38	574.6	555.99	565.52	572.3
1203.5	575.07	556.48	565.64	574.71
1221.73	575.62	559.85	566.36	575.42
1223.56	576.6	560.35	568.77	577.18
1229.88	589.68	594.3	600.8	598.84
1230.31	590.56	595.1	600.96	600.11
1271.04	601.04	597.75	601.84	600.3
1272.63	601.06	598.23	603.85	601.43
1274.65	619.03	630.7	635.72	614.32
1274.97	619.35	632.74	635.8	615.46
1279.85	620.58	632.85	636.25	615.72
1281.05	620.59	633.71	638.37	616.04
1282.61	620.68	641.45	641.04	628.05
1286.01	620.9	642.07	641.39	629.96
1349.41	623.27	642.59	641.68	631.38
1349.59	623.55	644.74	642.15	632.68
1360.79	668.28	644.96	647.02	656.16
1361.99	669	645.26	647.1	656.31
1390.63	670.9	645.63	648.99	656.71
1391.13	671.2	645.86	648.99	657.75
1395.05	678.56	676.78	680.58	659.41
1395.14	678.8	676.89	680.87	660.19
1402.91	679.4	677.41	682.14	661.07
1404.18	680.6	677.78	682.31	661.7
1410.02	699.95	711.65	716.37	704.83
1411.08	700	711.92	716.58	704.95
1414.01	702.24	712.03	717.15	705.57
1414.21	702.34	712.69	717.61	705.7
1443.75	712.37	712.93	717.63	708.28
1444.16	712.7	713.37	717.84	709.1
1467.03	713.74	713.52	719.25	709.43
1468.56	714.2	714.22	720.2	710.12
1474.93	722.15	731.68	728	713.07
1475	722.48	732.96	730.35	714.34
1477.27	724.74	733.97	731.45	714.69
1478.41	725.39	734.27	731.88	714.89
1482.65	734.36	734.47	736.65	735.81
1484.97	734.4	734.64	736.71	736.27
1485.49	736.54	737.83	736.93	736.31
1485.62	737.12	739.25	737.39	737.19
1494.14	778.47	775.45	785.67	802.35
				1501.48

1494.68	775.9	788.39	802.52
1534.23	779.54	794.64	802.96
1534.69	779.6	796.17	803.03
1540.05	815.3	807.82	807.59
1540.5	815.33	809.24	820.31
1577.71	816.1	810.85	822.67
1578.11	816.35	811.48	823.6
1619.04	826.2	838	839.81
1620.99	826.3	840.12	840.41
1632.15	826.33	841.34	840.5
1632.61	826.52	841.49	841.27
1655.29	829.01	844.02	842.04
1656.05	829.36	846.56	842.92
1668.71	840.99	850.71	845.27
1669	841.09	851.75	847.07
1742.37	847.6	854.58	852.03
1742.47	847.74	855.03	852.52
1748.93	848.18	864.41	853.4
1756.07	848.8	866.88	854.67
3069.51	869.89	867.04	858.12
3069.56	869.96	868.04	864.55
3070.52	880.54	869.51	866.35
3070.73	881	871.57	867.54
3136.22	890.82	872.65	867.66
3136.3	890.99	873.71	868.26
3136.69	894.34	887.26	872.55
3136.93	894.35	889.09	873.83
3192.02	895.58	911.46	925.71
3192.15	896.79	911.8	925.8
3193.73	898.46	912.52	926.03
3194.66	898.53	912.94	926.91
3195.14	972.44	931.99	938.06
3195.64	973.18	934.97	938.3
3196.27	973.59	935.38	938.36
3196.72	977	935.85	938.85
3216.41	981.23	975.46	973.81
3216.54	982.63	975.78	974.47
3218	986.8	975.82	975.66
3218.07	986.83	976.55	978.18
3226.19	992.95	977.21	979.62
3226.35	993.11	977.27	980.4
3228.31	998.92	977.89	981
3228.36	999.3	978.14	981.52
3259.32	1001.64	989.15	984.21

3259.46	991.68	988.17	981.78
3263.58	992.33	989.46	982.47
3263.81	992.59	996.29	983.73
1011.89	1005.84	996.65	1010.5
1012.34	1007.82	997.42	1010.68
1014.13	1008.64	999.17	1011.44
1014.45	1011.28	1000.07	1011.98
1015.08	1030.3	1004.28	1031.21
1016.83	1030.51	1006.09	1033.
1019.01	1031.3	1011.77	1035.47
1021.64	1032.62	1012.9	1035.78
1024.23	1032.98	1038.28	1040.67
1024.82	1033.68	1039.59	1041.
1032.63	1035.65	1040.12	1042.2
1033.28	1037.78	1041.39	1042.52
1043.27	1044.92	1044.63	1044.2
1043.29	1046.41	1044.79	1044.22
1043.94	1046.61	1044.94	1044.87
1044.4	1046.72	1045.47	1045.91
1044.73	1047.12	1056.4	1048.83
1045.28	1047.95	1057.14	1049.49
1045.88	1049.11	1059.33	1050.06
1046.81	1049.48	1059.46	1050.97
1082.38	1068.61	1071.5	1072.74
1083.29	1069.43	1071.89	1072.83
1085.77	1069.89	1072.01	1073.05
1086.82	1071.04	1072.25	1075.24
1145.89	1115.51	1116.02	1145.83
1146.72	1116.11	1116.06	1147.06
1148.97	1117.07	1116.34	1147.43
1149.31	1118.14	1117.04	1148.07
1161.52	1145.74	1150.06	1148.6
1161.65	1147.89	1150.32	1151.05
1164.08	1149.21	1150.36	1152.48
1178.6	1191.05	1179.43	1194.08
1176.06	1181.38	1177.1	1191.74
1177.63	1181.89	1177.11	1192.96
1178.15	1185.57	1178.78	1193.64
1178.6	1191.05	1179.43	1194.08
1192.05	1193.13	1193.63	1194.18
1192.27	1193.56	1194.59	1196.32
1197.98	1194.58	1196	1197.85
1198.31	1197.11	1196.11	1198.23
1207.14	1208.18	1213.52	1212.66

1207.39	1209.94	1213.59	1212.71
1210.13	1214.43	1213.72	1213.24
1210.2	1214.9	1215.27	1213.59
1233.68	1221.82	1219.66	1232.91
1234.06	1224.42	1221.97	1233.2
1241.87	1225.39	1222.51	1234.19
1242.28	1225.61	1222.72	1235.12
1243.06	1226.51	1229.1	1235.89
1243.87	1226.64	1229.16	1237.18
1250.44	1229.76	1229.17	1237.27
1250.66	1232.1	1230.42	1238.71
1263.37	1259.05	1258.99	1266.
1268.33	1260.81	1259.19	1267.68
1269.78	1261.23	1259.47	1268.59
1270.8	1261.36	1259.61	1269.09
1272.84	1277.92	1281.07	1270.94
1274.54	1280.26	1281.8	1271.49
1274.85	1280.72	1283.25	1271.89
1275.79	1281.29	1284.27	1272.38
1287.05	1282.01	1285.74	1272.63
1287.18	1283.56	1285.8	1273.8
1288.4	1285.58	1286.7	1274.95
1291.39	1286.24	1288.71	1275.81
1291.53	1287.38	1291.24	1292.47
1291.57	1287.54	1291.56	1292.69
1292.03	1287.82	1293.05	1293.69
1296.87	1287.89	1295.56	1293.85
1358.04	1358.83	1364.1	1351.51
1358.69	1361.4	1364.95	1352.26
1360.82	1362.19	1365.64	1352.52
1361.36	1362.31	1366.21	1353.36
1367.14	1377.09	1376.48	1365.32
1367.73	1377.54	1376.62	1365.78
1371.44	1378.42	1378.04	1367.56
1371.48	1380.06	1378.09	1368.15
1389.85	1391.83	1393.47	1387.81
1393.6	1391.92	1393.69	1388.78
1395.02	1393.68	1393.71	1391.29
1396.02	1394.58	1394.5	1391.35
1399.23	1395.93	1402.23	1393.43
1400.37	1396.55	1402.73	1394.44
1400.56	1397.21	1402.95	1396.26
1401.57	1398.5	1403.33	1397.97
1408.57	1403.34	1407.94	1404.56

1409.7	1404.23	1410.09	1404.92
1410.79	1404.9	1411.07	1404.99
1410.92	1405.02	1413.02	1406.13
1411.01	1416.23	1417.72	1411.17
1412.14	1416.52	1418.07	1411.25
1413.13	1416.53	1419.15	1411.5
1415.61	1417.05	1419.91	1412
1415.77	1432.67	1435.44	1431.23
1416.3	1432.98	1435.78	1431.37
1418.49	1434.03	1436.81	1431.38
1419.72	1434.97	1437.1	1431.77
1447.84	1456.13	1455.4	1451.84
1447.91	1456.38	1455.59	1451.85
1453.98	1456.38	1455.61	1452.62
1454.05	1456.78	1456.4	1452.83
1467.67	1456.82	1456.59	1469.98
1469.24	1457.74	1456.78	1470.19
1470.15	1457.81	1456.79	1470.23
1470.56	1458.82	1457.84	1470.38
1475.65	1473.3	1486.68	1478.76
1476.92	1473.46	1487.88	1479.1
1479.21	1473.72	1488.11	1479.21
1480.01	1475.33	1489.11	1479.69
1482.1	1478.81	1489.3	1485.63
1486.88	1479.09	1489.98	1485.95
1487.04	1480.37	1490.72	1486.09
1490.26	1482.15	1491.31	1486.15
1493.63	1484.51	1495.92	1489.38
1493.91	1484.54	1495.95	1489.42
1496.77	1484.78	1496.56	1489.54
1497.27	1485.15	1496.87	1490.95
1497.7	1498.57	1498.48	1495.81
1497.96	1498.81	1499.83	1496.86
1505.2	1499.22	1501.15	1497.31
1505.89	1500.48	1501.78	1497.77
1516.45	1504.75	1504.07	1499.88
1516.7	1504.83	1505.39	1500.12
1518.14	1506.35	1505.46	1500.19
1519.27	1506.52	1506.4	1500.66
1543.65	1527.37	1530.3	1537.25
1544.89	1527.39	1530.63	1537.92
1546.35	1527.48	1530.75	1538.16
1546.66	1527.91	1531.12	1538.92
1549.56	1539.64	1557.9	1546.04

1549.71	1559.84	1547.95	1546.88
1549.71	1559.9	1558.01	1547
1550.39	1560.8	1559.72	1547.62
1583.46	1561.12	1565.91	1580.95
1583.46	1561.36	1566.53	1581.29
1584.26	1561.84	1567.11	1581.34
1584.48	1561.97	1567.68	1581.59
1617.16	1629.55	1629.76	1611.69
1618.25	1629.7	1630.33	1612.15
1620.24	1629.93	1630.59	1612.19
1622.61	1630.65	1631.29	1612.39
1636.62	1633.57	1633.82	1637.01
1637.13	1633.82	1634.18	1638.2
1639.15	1634.01	1634.77	1638.79
1639.15	1634.57	1634.9	1638.95
1661.65	1656.98	1660.18	1657.94
1661.74	1657.59	1660.73	1658.42
1662.96	1658.11	1662.56	1658.68
1663.51	1658.14	1662.7	1658.74
1675.93	1672.57	1676.96	1670.86
1675.97	1672.68	1677.45	1671.52
1676.42	1672.94	1677.83	1671.54
1676.69	1674.29	1678.4	1672.23
1707.24	1732.24	1718.22	1728.06
1708.03	1735.9	1719.89	1728.1
1710.86	1739.4	1720.91	1734.19
1715.22	1740.15	1722.31	1735.18
1720.39	1743.36	1729.65	1736.11
1721.38	1744.45	1733.95	1737.11
1723.64	1744.54	1734.02	1737.49
1724.25	1757.11	1734.72	1737.81
3054.41	3068.87	3043.46	3060.2
3054.41	3068.87	3043.59	3060.2
3054.42	3069.04	3043.65	3060.38
3054.5	3069.06	3043.82	3060.39
3068.65	3069.12	3071.54	3067.72
3068.82	3069.42	3071.59	3067.83
3070.4	3069.5	3071.7	3067.84
3071.18	3069.76	3071.71	3067.89
3139.36	3140.55	3128.6	3141.16
3139.48	3140.59	3128.6	3141.22
3140.02	3140.74	3128.6	3141.3
3140.09	3140.83	3128.72	3141.33
3143.11	3140.98	3143.79	3147.75

3143.13	3141.07	3143.85	3147.79
3145.27	3141.25	3143.88	3147.8
3145.4	3141.26	3144.04	3147.81
3166.48	3195.78	3170.2	3188.67
3166.49	3195.81	3170.2	3188.71
3166.63	3195.83	3170.23	3188.73
3166.76	3195.97	3170.4	3188.73
3180.35	3198.95	3184.88	3191.56
3180.37	3199.14	3184.93	3191.64
3180.51	3199.19	3185.05	3191.68
3180.57	3199.28	3185.1	3191.72
3203.09	3214.27	3188.73	3197.63
3203.14	3214.28	3188.74	3197.78
3203.17	3214.9	3189.74	3197.8
3203.2	3215.04	3189.85	3197.81
3205.58	3217.66	3200.08	3203.12
3205.69	3217.72	3200.15	3203.26
3205.79	3218.07	3200.17	3203.26
3206.02	3218.07	3200.19	3203.29
3207.23	3224.18	3202.66	3204.77
3207.35	3224.27	3202.67	3204.77
3207.71	3224.4	3202.7	3205.64
3208.5	3224.56	3202.73	3205.67
3218.54	3224.57	3216.63	3209.09
3218.55	3224.6	3216.63	3209.1
3218.67	3224.94	3216.9	3209.22
3219.09	3224.95	3216.94	3209.33
3233.29	3236.25	3251.11	3229.63
3233.29	3236.4	3251.19	3229.85
3236.06	3236.51	3251.2	3229.91
3236.06	3236.51	3251.22	3230.01
3251.38	3240.64	3269.67	3252.07
3251.4	3240.87	3269.82	3252.3
3251.81	3241.16	3269.98	3252.57
3251.87	3241.17	3270.73	3252.96
3276.37	3281.76	3288.76	3275.61
3276.42	3281.79	3288.94	3275.63
3277.43	3281.82	3288.96	3275.78
3277.59	3281.87	3288.99	3275.81
3281.79	3283.14	3291.03	3289.11
3281.83	3283.26	3291.05	3289.14
3281.84	3283.27	3291.12	3289.35
3281.94	3283.39	3291.27	3289.57

Chapter S2

Crystal Structures of new polymorphs

S2.1 Crystal structures of 2'AP polymorphs

Both polymorphs crystallize in monoclinic system, phase α in $P2_1/n$ space group, while phase β in $P2_1/c$. The asymmetric unit of polymorph α contains only half of a molecule (the other half is generated by an crystallographic inversion), while, in the asymmetric unit of polymorph β there are halves of two distinct independent molecules (the other halves being generated by crystallographic inversions). In terms of molecular geometry, one of the molecules in 2'AP- β , denoted as B, is essentially the same as the one in α polymorph. Both of them have flat aromatic pyrene rings and carbonyl groups similarly tilted away from that plane by about 35 ° (Table S2.1). The molecule A in the polymorph β is essentially flat, with the carbonyl groups tilted out of pyrene plane by only about 1 ° (Table S2.1).

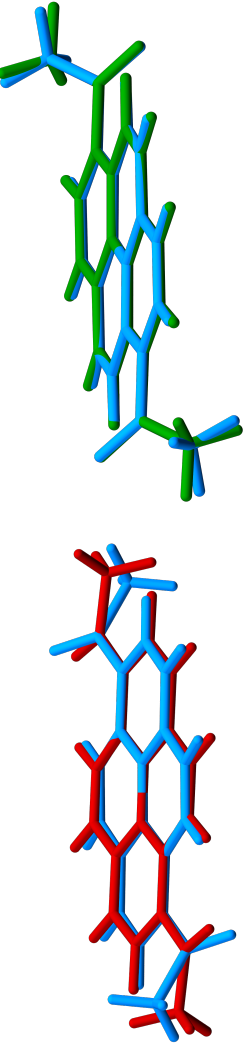


Figure S2.1: The best molecule overlays of molecule A (red) and B (green) of diacetyl-pyrene from the new β polymorph on a molecule from 2'AP- α polymorph (blue), as calculated with Mercury4[16].

Table S2.1: Geometry parameters of 2'AP structures.

	2'AP- α			2'AP- β			A		
	1 atm	0.5 GPa	1.8 GPa	1 atm	0.5 GPa	2.0 GPa	1 atm	0.5 GPa	2.0 GPa
Plane normal to plane normal angle:	35.75(3)	34.9(3)	33.2(4)						
Plane to plane twist angle:	32.25(5)	31.2(4)	28.8(6)	6.45(6)	6.2(2)	5.5(8)			
Plane to plane fold angle:	61.83(7)	61.2(6)	58.4(9)	3.70(3)	3.49(11)	2.6(4)			
torsion angle:	-36.64(17)	-35.0(18)	-43(4)	-34.61(19)	-37.0(7)	37(2)	-0.9(2)	-3.0(10)	-9(2)
Plane A centroid to plane B centroid:				3.78120(5)	3.6845(15)	3.449(6)			
Plane A to plane B centroid:				3.5055(5)	3.408(2)	3.182(8)			
Plane A to plane B shift:				1.4174(11)	1.400(5)	1.330(15)			
Plane B to plane A centroid distance:				-3.4415(4)	-3.351(2)	-3.157(7)			
Plane B to plane A shift:				1.5664(10)	1.531(5)	1.387(13)			

The crystal structure of α polymorph has been already described by Rajagopal et al.[4]. The main packing motif of α polymorph consists of tapes of molecules along [1 0 -1] direction connected by C–H \cdots π interactions. C–H \cdots π interactions also connect molecules in the neighboring tapes, creating herringbone packing. In [001] direction molecules also form tapes, connected by C–H \cdots O interactions.

In the structure of new β polymorph tapes of molecules can also be distinguished. Such motif is occurring along three different directions - [010], [100] and [1 0 -1]. Similarly to polymorph α , molecules in tapes along [010] direction are connected by C–H \cdots O interactions. Structure of polymorph β consist of independent molecules A and B and a molecule of one type is surrounded by six molecules of the other type. Therefore, in tapes along [010] and [1 0 -1] directions two types of molecules are arranged alternately, while tapes along \vec{a} direction only consist of molecules of the same type.

Most importantly, molecules of diacetyl-pyrene in 2'AP- β form π -stacks along [001] direction, in which molecules A and B alternate exactly one above the other; differences in molecular geometries making the resulting π -stacking more condensed. The molecules in a stack are additionally connected by C–H \cdots O interactions (Figure S3.4 and S3.5).

S2.1.1 Evolution of crystal structures of 2'AP with increased pressure

Neither 2'AP polymorph showed indications of phase transition in tested pressure range (up to about 2 GPa) judging by the systematic extinction patterns (Figures S2.2 and S2.3).

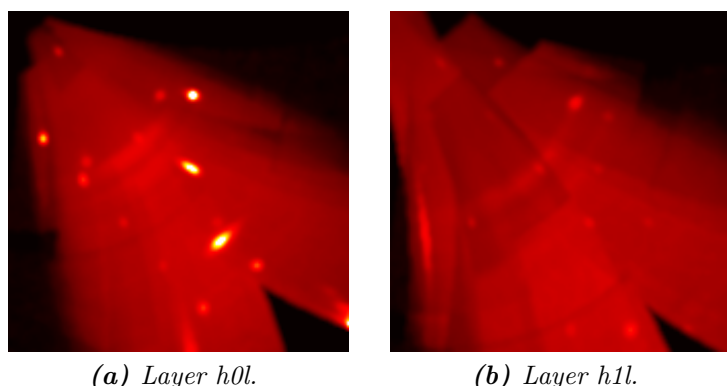


Figure S2.2: Layers $h0l$ and $h1l$ for 2'AP- α high-pressure experiment in 1.69 GPa. Differences between the layers confirm the presence of systematic extinctions at $h+l=2n+1$, consistent with the $n_{[010]}$ glide plane

Under the influence of pressure, the unit cells of both polymorphs are evenly compressed and that is the only observed effect (Figure S2.4). This is different than for 2°AP- α and 2"AP- α polymorphs, where applying pressure caused molecules to tilt from their original position.

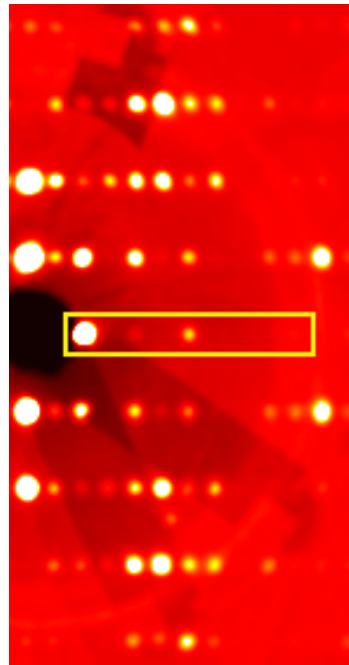


Figure S2.3: Layer $0kl$ for 2'AP- β high-pressure experiment in 1.98 GPa. Axis $0k0$, in which systematic extinctions $l=2n+1$ from $c_{[010]}$ glide plane are visible, was marked by yellow box.

Table S2.2: Estimated compression of unit cell parameters under pressure.

	Pressure [GPa]	a [%]	b [%]	c [%]	V [%]
2'AP- α	1.8	2.2	4.5	2.1	9.3
2'AP- β	2.0	2.7	2.0	8.8	13.2

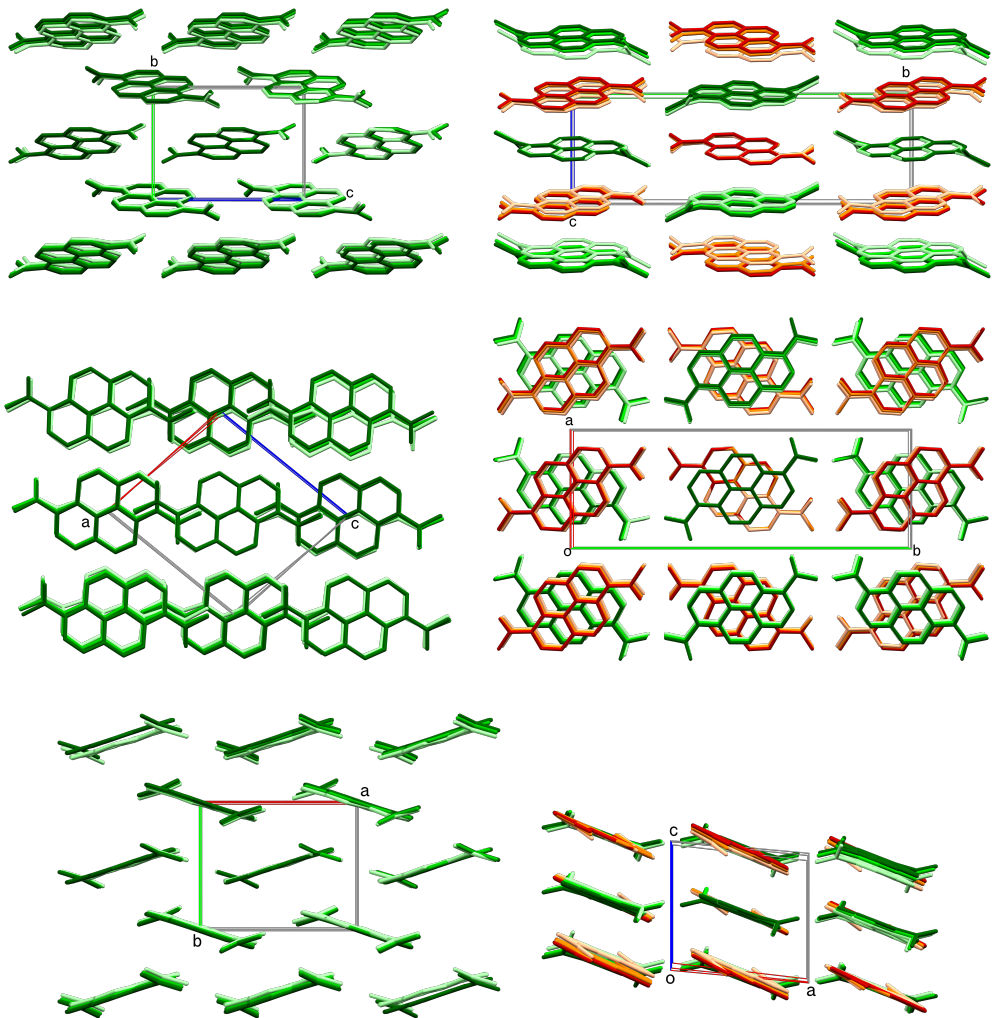


Figure S2.4: Crystal structure overlays of 2'AP- α (left) and 2'AP- β (right) from atmospheric conditions and increased pressures. Molecule A and B of 2'AP- β represented in red and green accordingly. Higher pressure indicated by lighter stick shades. Structure overlays calculated with Mercury4[16] based on crystallographic asymmetric unit.

Chapter S3

Lattice interactions

S3.1 The most important intermolecular interactions

Estimation of intermolecular interaction energy for all diacetyl-pyrene crystal forms have been performed in CrystalExplorer17[24], using cluster DFT/B3LYP calculations and standard 6-31G** database. The cluster included all molecules whose closest distance to the central molecule was below 3.8Å. Initial geometry in all cases was based on crystal structures determined at 100K. Obtained values of interaction energies are summarized in Tables ?? and ??.

Both polymorphs of 2'AP present more uniform networks of intermolecular interactions than other diacetyl-pyrene isomers. Their interactions form rectangular patterns and occurs mostly along main crystallographic directions or their diagonals.

In all β polymorphs there are stacks of molecules with π -stacking interactions. In the structure of 2°AP- β it is possible to distinguish two types of this interactions. One them is the strongest interaction in all of discussed compounds and have an energy of -73.6 kJ/mol. The other one is weaker and have an energy of -63.4 kJ/mol. The π -stacking interaction in the structure of 2'AP- β has an energy of -68.5 kJ/mol, while this type of interaction in the 2"AP- β is the weakest and have the energy of -58.5 kJ/mol. The only other significant interactions in the β polymorphs are C–H…O interactions. They arrange in hexagonal networks in the structures of 2°AP- β and 2"AP- β and a rectangular one in 2'AP- β .

Tapes of CH- π interactions are the main motif in the structures of all α polymorphs. The strongest ones also occur in 2°AP- α (-60.0 kJ/mol). There are also C–H…O interactions connecting molecules from subsequent tapes, all of similar strength (\approx 20 kJ/mol).

Intermolecular interaction networks of 2"AP- α and 2°AP- α - the materials prone to pressure-induced phase transformations - appear less dense than of 2'AP- α ; it is possible to find 'voids' in which there are no strong interactions, allowing for tilting of the molecules. In the structure of 2'AP- α there are no such 'voids' and interactions of comparable strength are uniformly distributed in all crystallographic directions. Therefore, a single molecule in 2'AP- α is more consistently stabilized than single molecules in 2"AP- α and 2°AP- α and has literally no room to change its orientation.

Table S3.1: Intermolecular interactions in 2° AP- α found between molecules within 3.8\AA range.

Symmetry operation	Distance [Å]	Energy [kJ/mol]				Total
		Electrostatic	Polarization	Dispersion	Repulsive	
$x+1/2, -y+1/2, -z+1/2$	8.62	-2.5	-0.7	-28.9	12.8	-20.4
$-x+1/2, -y, z+1/2$	10.30	-1.2	-0.5	-9.9	4.3	-7.6
$x+1/2, -y+1/2, -z+1/2$	5.1	-14.8	-5	-77.9	44	-60
x, y, z	11.34	-0.2	-0.9	-17.3	10.5	-9.5
$-x, -y, -z$	8.74	-15.3	-4.1	-18.8	16.1	-25.7
$-x, -y, -z$	12.51	-3.6	-0.8	-6.6	0	-10.2

Table S3.2: Intermolecular interactions in 2° AP- β found between molecules within 3.8\AA range.

Symmetry operation	Distance [Å]	Energy [kJ/mol]				Total
		Electrostatic	Polarization	Dispersion	Repulsive	
x, y, z	11.16	-4.8	-1.1	-7.8	4.4	-9.9
$-x, -y, -z$	3.81	-10.6	-2.4	-93.2	49.7	-63.4
$-x+1/2, y+1/2, -z+1/2$	10.04	-11.7	-3.1	-16.2	13.4	-20.5
$x+1/2, -y+1/2, z+1/2$	10.04	-0.9	-1.4	-14.9	6.7	-10.8
$-x+1/2, y+1/2, -z+1/2$	10.77	-2.5	-0.4	-10.2	6.8	-7.6
$-x, -y, -z$	10.91	-3.6	-0.9	-10.6	4.7	-10.8
$x+1/2, -y+1/2, z+1/2$	10.99	-1.6	-1.2	-11.3	8.9	-6.9
$-x, -y, -z$	3.69	-12	-4.4	-108.7	60	-73.6

Table S3.3: Intermolecular interactions in $2''$ AP- α found between molecules within 3.8\AA range.

Symmetry operation	Distance [Å]	Energy [kJ/mol]				Total
		Electrostatic	Polarization	Dispersion	Repulsive	
$-x, y+1/2, -z+1/2$	11.66	0.2	-0.9	-16.2	9.5	-8.6
$x, -y+1/2, z+1/2$	7.13	-8	-3.3	-51.6	27.3	-38.9
$-x, -y, -z$	8.86	-3.2	-1.3	-17.6	7.1	-15.3
$-x, -y, -z$	6.23	-11.5	-1.7	-62.7	33	-47.6
$x, -y+1/2, z+1/2$	10.67	-8.2	-2.3	-11	11.3	-13
$-x, y+1/2, -z+1/2$	13.41	-2.5	-0.4	-4.3	1.5	-5.8
$-x, -y, -z$	7.36	-12.8	-2.5	-46.2	23.4	-41.1
x, y, z	8.19	-9.4	-2.8	-20.4	14	-21.1
$-x, -y, -z$	11.86	1.6	-0.2	-2.1	0	-0.2

Table S3.4: Intermolecular interactions in $2''$ AP- β found between molecules within 3.8\AA range.

Symmetry operation	Distance [Å]	Energy [kJ/mol]				Total
		Electrostatic	Polarization	Dispersion	Repulsive	
$x+1/2, y, z+1/2$	8.44	-6.4	-1.8	-19.8	13.7	-16.9
$-x+1/4, y+3/4, z+3/4$	9.84	-4.8	-2.6	-16.2	11.6	-13.9
x, y, z	4.69	-10.9	-3.4	-91.9	57.5	-58.5
$-x+1/4, y+3/4, z+3/4$	10.39	1.1	-0.4	-10.7	6	-4.8
$-x+1/4, y+1/4, z+1/4$	10.39	1.1	-0.4	-10.7	6	-4.8

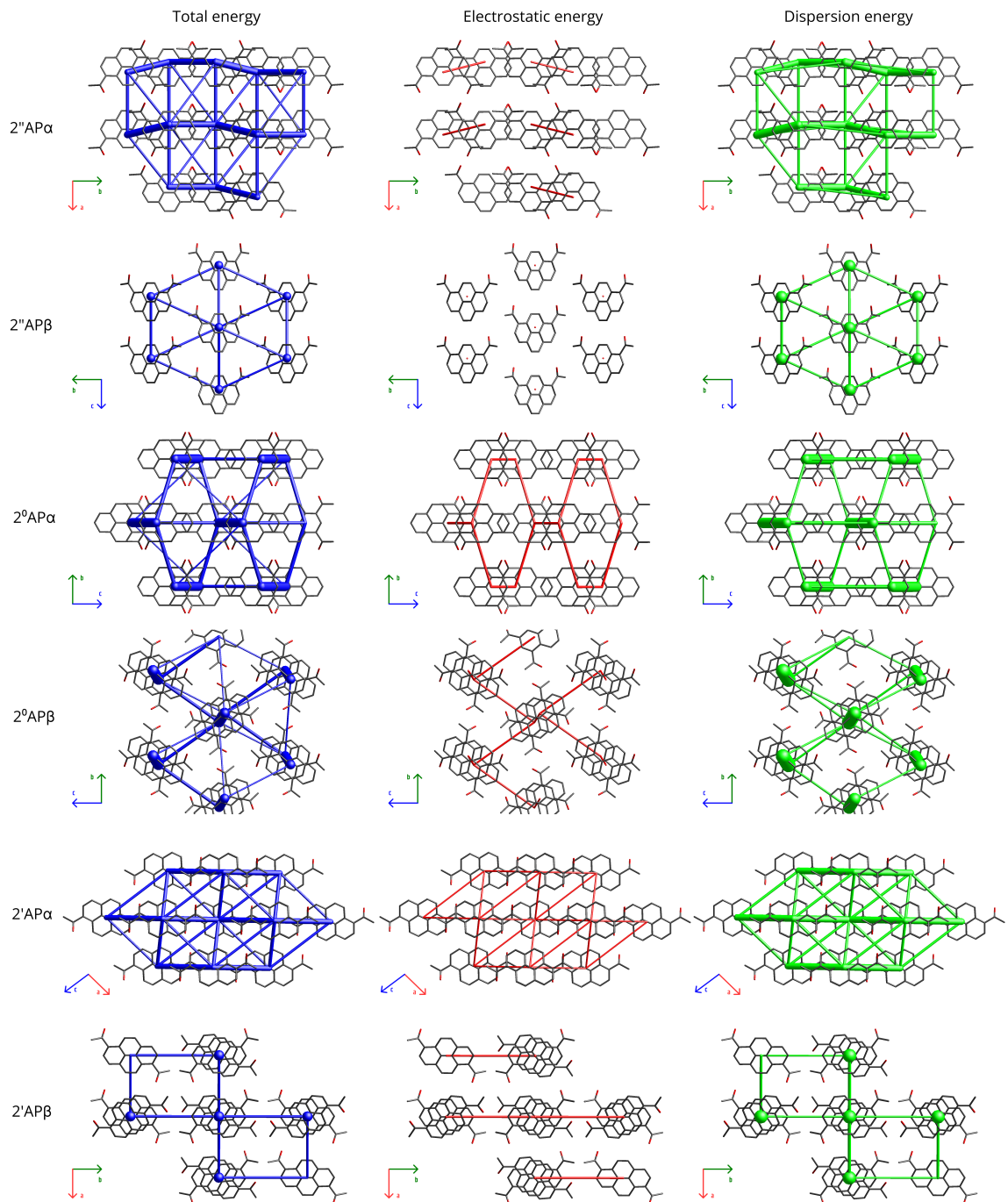


Figure S3.1: Crystal packing of diacetyl-pyrene polymorphs seen from direction along main motif. Energy frameworks calculated with *CrystalExplorer17* are overlaid on the crystal packing motifs. Blue tubes represent the total intermolecular interaction energies more negative than -10 kJ mol^{-1} and their thickness is scaled by the $|E|$.

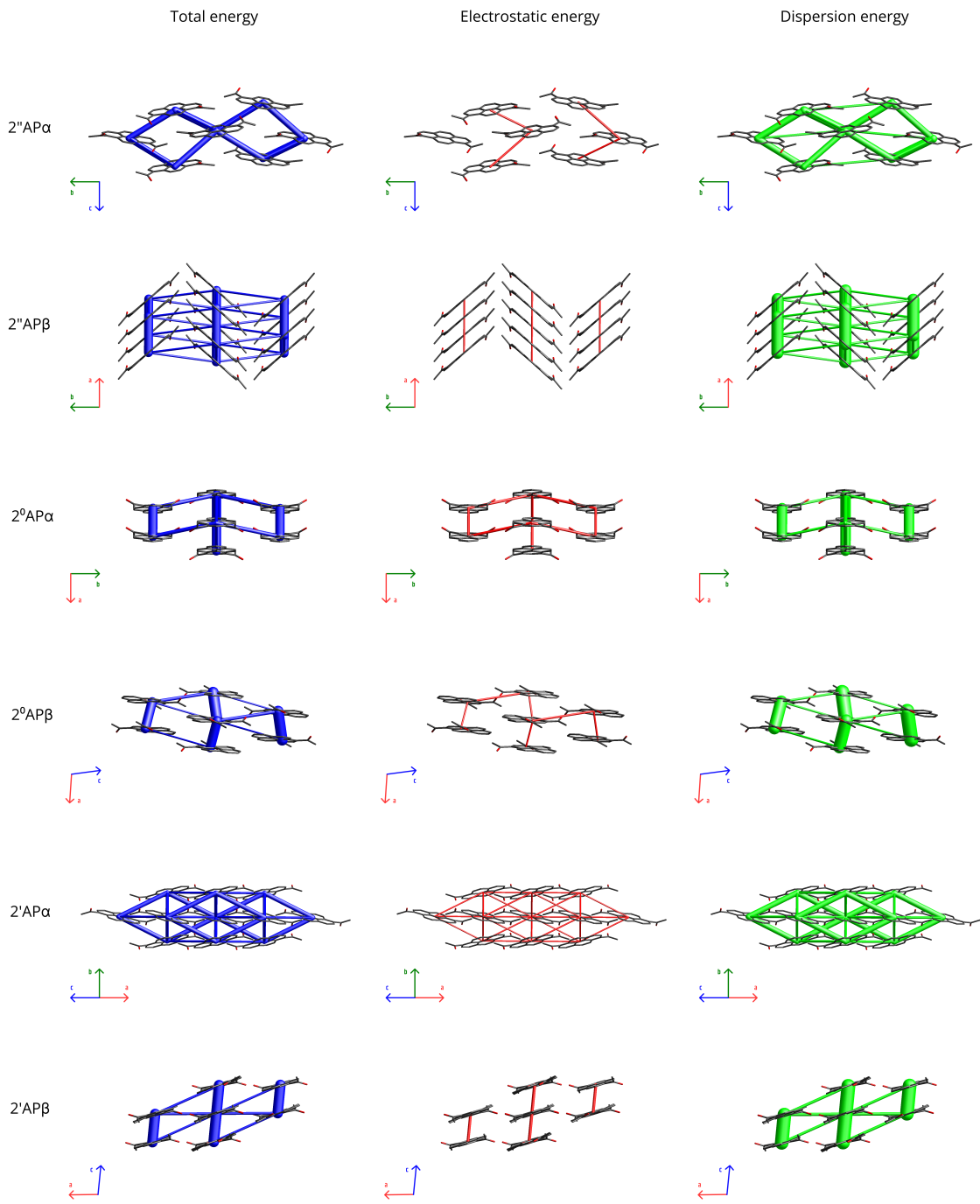


Figure S3.2: Crystal packing of diacetyl-pyrene polymorphs seen from one arbitrary direction. Energy frameworks calculated with CrystalExplorer17 are overlaid on the crystal packing motifs. Blue tubes represent the total intermolecular interaction energies more negative than -10 kJ mol^{-1} and their thickness is scaled by the $|E|$.

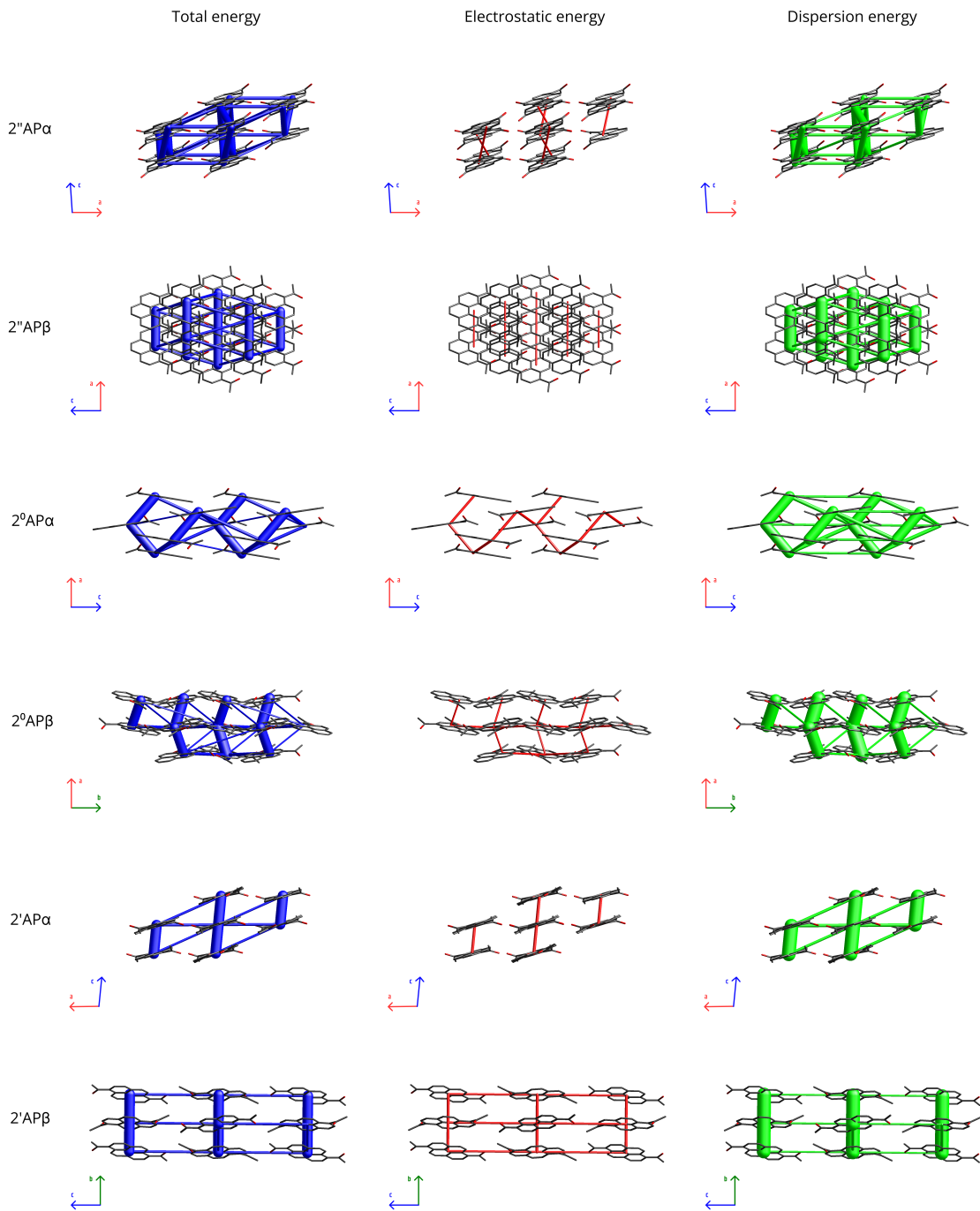


Figure S3.3: Crystal packing of diacetyl-pyrene polymorphs seen from another arbitrary direction. Energy frameworks calculated with CrystalExplorer17 are overlaid on the crystal packing motifs. Blue tubes represent the total intermolecular interaction energies more negative than -10 kJ mol^{-1} and their thickness is scaled by the $|E|$.

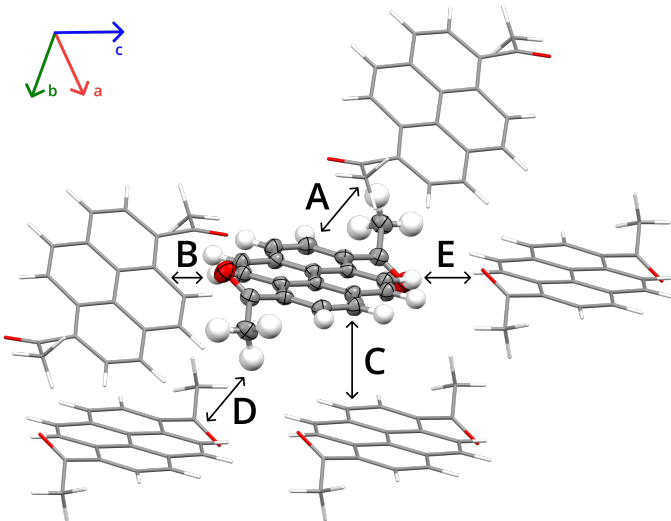


Figure S3.4: Scheme of interactions in the structure of 2'AP- α with symbols used in Table below.

Table S3.5: Intermolecular interactions in 2'AP- α found between molecules within 3.8 Å range.

	Symmetry operation	Distance [Å]	Energy [kJ/mol]				Total
			Electrostatic	Polarization	Dispersion	Repulsive	
A	-x+1/2, y+1/2, -z+1/2	8.19	-10.2	-2.8	-50.1	34.5	-35.2
B	-x+1/2, y+1/2, -z+1/2	7.26	-10.3	-2.8	-20.8	13.3	-22.8
C	x, y, z	9.2	-2	-1	-21.3	11.2	-14.5
D	x, y, z	14.67	-0.5	-0.1	-7.2	0	-6.9
E	x, y, z	10.08	-9.7	-4.1	-19.6	21.6	-17

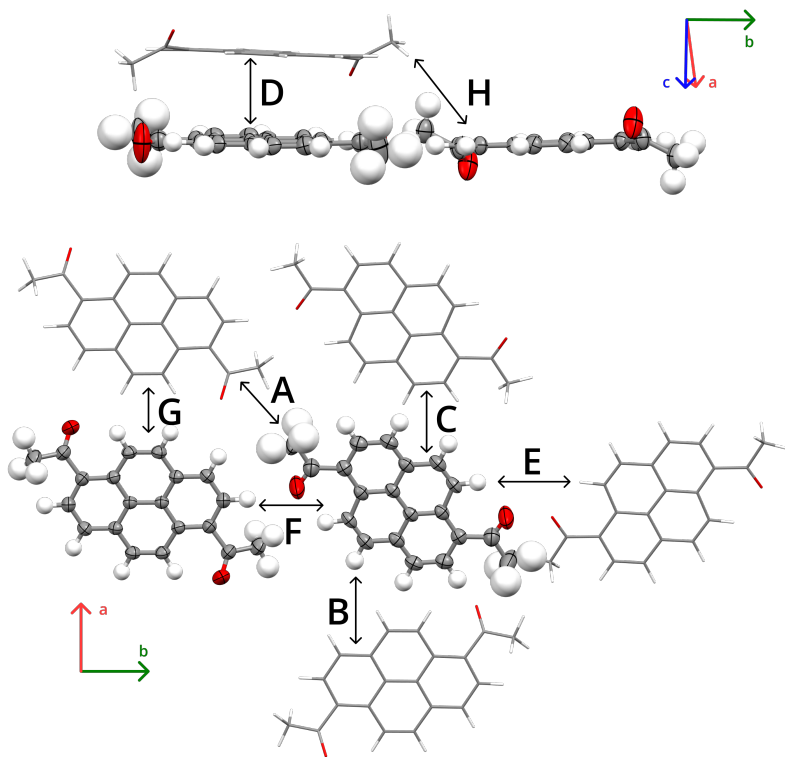


Figure S3.5: Scheme of interactions in the structure of 2'AP- β with symbols used in Table below.

Table S3.6: Intermolecular interactions in 2'AP- β found between molecules within 3.8\AA range.

Symmetry operation	Distance [\AA]	Energy [kJ/mol]				Total	
		Electrostatic	Polarization	Dispersion	Repulsive		
A	-	14.09	0.6	-0.5	-4.9	0	-4
B	-	9.19	-4.5	-1.8	-20.9	14.7	-15.2
C	x, y, z	8.03	-6	-1	-24.3	17.2	-17.6
D	-	3.73	-17.4	-2.8	-102.8	67.2	-68.5
E	-x, y+1/2, -z+1/2	12.16	3.2	-0.7	-6.3	0	-2.6
F	-	11.58	-13.3	-3.8	-14.3	20.2	-16.8
G	x, y, z	8.03	-15.2	-4.5	-23.2	18	-28.5
H	-x, y+1/2, -z+1/2	12.16	-0.1	-0.6	-8.2	0	-7.7

Bibliography

- (1) Tchoń, D.; Trzybiński, D.; Wrona-Piotrowicz, A.; Makal, A. *CrystEngComm* **2019**, *21*, 5845–5852.
- (2) Tchoń, D.; Bowskill, D.; Sugden, I.; Piotrowski, P.; Makal, A. *Journal of Materials Chemistry C* **2021**, *9*, 2491–2503.
- (3) Zwolenik, A.; Tchoń, D.; Makal, A. *IUCrJ* **2024**, *11*, DOI: 10.1107/S2052252524003634.
- (4) Rajagopal, S. K.; Philip, A. M.; Nagarajan, K.; Hariharan, M. *Chemical Communications* **2014**, *50*, 8644–8647.
- (5) Rigaku-Oxford-Diffraction CrysAlisPro Software System, version 1.171.38.46, Rigaku Oxford Diffraction, 2019.
- (6) Tchoń, D. pRuby: Python library for calculating pressure based on Ruby fluorescence (2021), University of Warsaw., 2021.
- (7) Piermarini, G. J.; Block, S.; Barnett, J. D.; Forman, R. A. *Journal of Applied Physics* **1975**, *46*, 2774–2780.
- (8) Ragan, D. D.; Gustavsen, R.; Schiferl, D. *Journal of Applied Physics* **1992**, *72*, 5539–5544.
- (9) Sheldrick, G. M. *Acta Crystallographica Section A: Foundations and Advances* **2015**, *71*, 3–8.
- (10) Bourhis, L. J.; Dolomanov, O. V.; Gildea, R. J.; Howard, J. A. K.; Puschmann, H. *Acta Crystallographica Section A: Foundations and Advances* **2015**, *71*, Number: 1 Publisher: International Union of Crystallography, 59–75.
- (11) Kleemiss, F. et al. *Chemical Science* **2021**, *12*, 1675–1692.
- (12) Chodkiewicz, M. L.; Migacz, S.; Rudnicki, W.; Makal, A.; Kalinowski, J. A.; Moriarty, N. W.; Grosse-Kunstleve, R. W.; Afonine, P. V.; Adams, P. D.; Dominiak, P. M. *Journal of Applied Crystallography* **2018**, *51*, 193–199.
- (13) Sheldrick, G. M. *Acta Crystallographica Section C-Structural Chemistry* **2015**, *71*, WOS:000347804100002, 3–8.
- (14) Sheldrick, G. M. *Acta Crystallographica Section D: Biological Crystallography* **2010**, *66*, Number: 4 Publisher: International Union of Crystallography, 479–485.
- (15) Dolomanov, O. V.; Bourhis, L. J.; Gildea, R. J.; Howard, J. A. K.; Puschmann, H. *Journal of Applied Crystallography* **2009**, *42*, 339–341.

- (16) Macrae, C. F.; Bruno, I. J.; Chisholm, J. A.; Edgington, P. R.; McCabe, P.; Pidcock, E.; Rodriguez-Monge, L.; Taylor, R.; van de Streek, J.; Wood, P. A. *Journal of Applied Crystallography* **2008**, *41*, 466–470.
- (17) Groom, C. R.; Bruno, I. J.; Lightfoot, M. P.; Ward, S. C. *Acta Crystallographica Section B* **2016**, *72*, 171–179.
- (18) Dovesi, R.; Erba, A.; Orlando, R.; Zicovich-Wilson, C. M.; Civalleri, B.; Masschio, L.; Rérat, M.; Casassa, S.; Baima, J.; Salustro, S.; Kirtman, B. *WIREs Computational Molecular Science* **2018**, *8*, e1360.
- (19) Grimme, S.; Antony, J.; Ehrlich, S.; Krieg, H. *The Journal of Chemical Physics* **2010**, *132*, 154104.
- (20) Grimme, S.; Ehrlich, S.; Goerigk, L. *Journal of Computational Chemistry* **2011**, *32*, 1456–1465.
- (21) Brandenburg, J. G.; Grimme, S. *Topics in current chemistry* **2014**, *345*, 1–23.
- (22) Brandenburg, J. G.; Alessio, M.; Civalleri, B.; Peintinger, M. F.; Bredow, T.; Grimme, S. *The journal of physical chemistry A* **2013**, *117*, 9282–9292.
- (23) Madsen, A. *Journal of Applied Crystallography* **2006**, *39*, Publisher: International Union of Crystallography, 757–758.
- (24) M. J. Turner; J. J. McKinnon; S. K. Wolff; D. J. Grimwood; P. R. Spackman; D. Jayatilaka; M. A. Spackman CrystalExplorer17 (2017), University of Western Australia., 2017.